Structural Characterization of Distinct α3N and α5 Metal Sites in the Cyanobacterial Zinc Sensor SmtB†

Michael L. VanZile, Xiaohua Chen, and David P. Giedroc*

Department of Biochemistry and Biophysics, Center for Advanced Biomolecular Research, Texas A&M University, College Station, Texas 77843-2128

Received March 1, 2002; Revised Manuscript Received May 30, 2002

ABSTRACT: SmtB is required for *Synechococcus* to effect a response to toxic concentrations of Zn(II) and other heavy metals. Direct binding of inducing metal ions to SmtB transcriptionally derepresses the expression of SmtA, a prokaryotic class II metallothionein. Homodimeric SmtB binds one Zn(II) or Co(II) per monomer in a cysteine thiolate-containing site in a tetrahedral coordination geometry [VanZile, M. L., et al. (2000) *Biochemistry 39*, 11818−11829]. In this report, characterization of a set of cysteine substitution mutants of SmtB reveals that SmtB homodimer binds Zn(II) or Co(II) in one of two mutually exclusive metal binding sites, termed α3N and α5, with very high equilibrium affinities. Both sites are characterized by similar affinities for Co(II) ($K_{Co} \approx 2-5 \times 10^9$ M^{-1}), while the Zn(II) affinities are at least 20-fold different ($K_{Zn}^{\alpha 3N} \geq 10^{13}$ M^{-1}; $K_{Zn}^{\alpha 5} \approx 5 \times 10^{11}$ M^{-1}). Co(II) bound exclusively at the α5 sites is capable of rapid equilibration between the α3N and α5 sites upon reduction of the mixed disulfides in S-methylated SmtB. These results suggest that the α3N or α5 metal sites might play distinct roles in this Zn(II)-sensing protein, systematically investigated in the following paper [VanZile, M. L., Chen, X., and Giedroc, D. P. (2002) *Biochemistry 41*, 9776−9786]. Since both the α3N and α5 sites are present in many members of the SmtB/ArsR family of metal sensor proteins, the presence of these two metal binding sites may explain some of the functional diversity in metal responses across this family of proteins.

Metal ions play important roles in many cellular processes as either structural components or cofactors in enzyme-catalyzed reactions (*1*, *2*). However, not all metals are beneficial for cellular growth, and even those that are become toxic at high concentrations. To alleviate the toxic effects of metal ion stress, homeostatic machinery has evolved to maintain the appropriate bioavailable intracellular concentration of essential metal ions while removing nonbeneficial heavy metal pollutants (*3*, *4*). The expression of much of this machinery is controlled by metal-sensing proteins at the transcriptional level. For example, a family of closely related prokaryotic transcriptional repressors, termed the ArsR/SmtB family, regulates the expression of genes associated with metal sequestration or efflux in both Gram-positive and Gram-negative bacteria (*5*, *6*).

Synechococcus PCC7942 SmtB is a founding member of the ArsR/SmtB family of metalloregulatory proteins that regulates the expression of the *smt* operon, which plays a role in zinc and cadmium resistance in the cyanobacterium *Synechococcus* (for a review, see ref *6*). The *smt* operon contains two divergently transcribed genes, *smtB* and *smtA*. SmtA is a class II metallothionein that functions in the direct sequestration of zinc ions (*7*, *8*). SmtB is a homodimeric *trans*-acting transcriptional repressor (*9*) that represses *smtA* transcription in the absence of heavy metals (*10*). Early reports showed that *smtA* gene expression is derepressed in the presence of Zn(II), Cd(II), and Cu(II), and to a lesser extent by Co(II) and Ni(II) (*10*); more recent studies suggest that SmtB functions primarily as a Zn(II) sensor in cyanobacteria.[1]

SmtB is a dimeric protein that directly associates with metal ions (*11*, *12*). We recently showed that homodimeric SmtB binds one metal ion per monomer (two per homodimer) and that the binding affinity for Zn(II) is very high ($K_{Zn} > 10^{11}$ M^{-1}) (*12*). Optical spectroscopy of Co(II)-substituted SmtB and Zn(II)- and Co(II)-EXAFS revealed that the metal coordination environment is tetrahedral or distorted tetrahedral, and contains one or two cysteine residues with at least one carboxylate and one imidazole ligand (*12*).

The X-ray crystallographic structure of apo-SmtB reveals that the monomer adopts a $\alpha\alpha\alpha\alpha\beta\beta\alpha$-fold to form a nearly 2-fold symmetric, highly elongated homodimer (*9*). The dimerization domain is primarily formed by the C-terminal α5 helix, although the two monomers are highly interdigitated. Difference electron density maps generated prior to crystal dissolution upon soaking apo-SmtB crystals with mercuric acetate suggested *two* pairs of symmetry-related metal binding sites per dimer, or four bound metals total (*9*), rather than just the two observed in solution (*12*). Despite very low occupancies (≤2%) and poor coordination geometries, one Hg(II) appeared to be ligated to Cys61 and Asp64

† This work was supported by grants from the NIH (GM42569) and the Robert A. Welch Foundation (A-1295).

* To whom correspondence should be addressed. E-mail: giedroc@tamu.edu. Telephone: (979) 845-4231. Fax: (979) 862-4718.

[1] J. S. Cavet, M. L. VanZile, W. Meng, M. A. Pennella, R. J. Appelhoff, D. P. Giedroc, and N. J. Robinson, manuscript submitted for publication.

10.1021/bi0201771 CCC: $22.00
Published on Web 07/10/2002

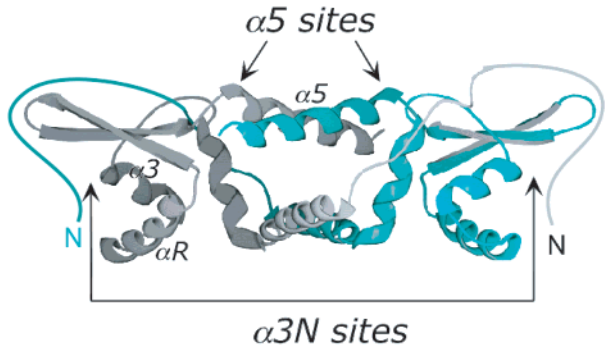

FIGURE 1: Ribbon representation of the structure of the apo-SmtB homodimer (*9*). Four metal binding sites were inferred from difference electron density maps calculated after soaking the crystals in mercuric acetate. Two symmetry-related sites were found bridging the α5 helices (denoted α5), and two others were found close to the α3 helix (denoted α3N). The N-terminal regions of each subunit (arms) (residues 1−24) were not observed in the structure (*9*) and are sketched as unstructured ribbons. The N-terminal arm of one subunit is close to the α3 helix of the other subunit (cf. Figure 5 below).

from helix α3, His97 from helix β2, and possibly a water molecule. The second Hg(II) site was determined to contain two residues derived from the α5 helix of each monomer of the protein: Asp104 and His106 from monomer A and His117′ and Glu120′ from monomer B (*9*) (see Figure 1; vide infra).

Functional characterization of mutant SmtBs reveals that none of the cysteine residues are absolutely required for Zn(II)-mediated transcriptional regulation in vivo and only His105 and/or His106 in the α5 helices was found to be essential (*13*). These experiments did show that T11S/C14S SmtB appeared to be less Zn(II)-inducible than wild-type SmtB, suggesting a possible role for Cys14 in regulation (*13*). Unfortunately, Cys14 is in the N-terminal region of SmtB that was not well ordered in the crystal structure (*9*). In addition, the C61S mutant appeared to be a poorer repressor in vivo, but was fully metal-responsive (*13*).

Since some subset of the three cysteine residues in SmtB clearly form part of the high-affinity Zn(II) complex in SmtB (*12*) yet appear *not* to be required for Zn(II) regulation in vivo (*13*), we have characterized the metal binding properties (this work) and DNA binding properties (*14*) of single and double nonliganding Cys → Ser mutants, S-methylated SmtB, and H106Q SmtB in an attempt to resolve this apparent paradox. We make the surprising finding that although the SmtB homodimer contains two pairs of structurally distinct metal binding sites, termed α3N and α5, only one-half of the sites can be bound to metal in solution, in a manner dictated by K_{Zn} and K_{Co} for these sites. The α3N metal binding site is structurally analogous to the Cd(II)/Pb(II)/Bi(III) site recently characterized in *Staphylococcus aureus* pI258 CadC (*15*−*17*), while the α5 metal binding site is highly conserved among the Zn(II)-sensing transcription factors in the ArsR/SmtB family, including *S. aureus* CzrA (*18*, *27*) and *Synechocystis* ZiaR (*19*). We also show that Co(II) bound in the C-terminal α5 site readily re-equilibrates between the α3N and α5 sites upon reversal of the mixed R-Cys-S-S-CH_3 disulfides in S-methylated SmtB with dithiothreitol, in a manner dictated by the equilibrium affinities of Co(II) for each of the two sites.

MATERIALS AND METHODS

Chemicals. All buffers were prepared using Milli-Q distilled deionized water. MES, HEPES, and Tris buffer salts were obtained from Sigma. All chromatography materials were obtained from Pharmacia Biotech. Ultrapure cobalt(II) chloride and zinc sulfate were obtained from Johnson-Matthey. Mag-fura-2 and quin-2 were obtained from Molecular Probes. The QuikChange mutagenesis kit was obtained from Stratagene.

Overexpression and Purification of Variant SmtBs. All mutants of SmtB were generated using the protocol supplied with the QuikChange kit. Generation of the single cysteine to serine mutations was carried out using the wild-type expression plasmid (pSRK15-1) (*11*) as a template for PCR and the appropriate mutagenic primers. Double mutants were generated using a previously mutated wild-type expression plasmid as a PCR template and the appropriate primers. For example, an expression construct designed to express C14S/C61S SmtB was generated using the C14S SmtB expression plasmid as a template and the C61S mutagenic primers. The C61S/C121S double mutant was constructed using the C121S SmtB expression plasmid as a template and the C61S mutagenic primers. Both strands of all expression constructs were completely sequenced to verify the integrity of the plasmids. All mutant SmtBs were purified in a manner essentially identical to that of wild-type SmtB (*12*). The S-methylated variant of wild-type SmtB was generated by reacting wild-type SmtB with 15 molar equiv of methylmethanethiosulfonate (MMTS) for 1 h at room temperature (*20*). The resulting protein was exhaustively dialyzed against buffer S [10 mM HEPES and 0.15 M KCl (pH 7.4)] to remove unreacted MMTS. All SmtB variants were determined to contain the expected number of reduced cysteine residues per mole (≈2 for the single mutants, ≈1 for the double mutants, and no free thiolates for the S-methylated protein) by DTNB reactivity and to be zinc-free (≤0.1 molar equiv of metal) by atomic absorption spectroscopy (*12*). C14S, C61S, and wild-type SmtBs were further subjected to N-terminal sequencing by the Protein Chemistry Laboratory at Texas A&M University to confirm the expected N-terminal sequences. The concentration of the SmtB monomer was determined for all variants using an ϵ_{280} of 5960 M^{-1} cm^{-1} (*12*).

Co(II) Binding Experiments. All metal binding experiments were carried out as previously described (*12*) except that they were performed under aerobic conditions. For the DTT recovery experiment, 66 μM Co(II)-substituted S-methylated SmtB [prepared 1:1 Co(II)/SmtB monomer mixture] was titrated aerobically at room temperature with a concentrated stock solution of DTT and incubated for 5 min, and the absorption spectrum was recorded as described previously (*12*). Under these solution conditions as well as those below, SmtB is largely dimeric as defined by a monomer−dimer equilibrium constant of 3.5×10^5 M^{-1} for apo-SmtB and 1.3×10^7 M^{-1} for Zn(II)-saturated SmtB (*11*).

Zn(II) Binding Experiments. Two different zinc chelator indicator dyes were used as apo-SmtB competitors: mag-fura-2 ($K_{Zn} = 5.0 \times 10^7$ M^{-1} at pH 7.0 and 25 °C) (*21*) and quin-2 ($K_{Zn} = 2.70 \times 10^{11}$ M^{-1}) (*22*). Mag-fura-2 competition experiments were carried out as previously described (*12*). For quin-2 competition assays, a known concentration

of quin-2 (20−30 μM) was mixed with a known concentration of apoprotein (20−40 μM) in 0.8 mL of buffer S and the optical spectrum was recorded from 240 to 800 nm. Following each *i*th addition of $ZnSO_4$ (2.5−10 μL), the reaction mixture was allowed to equilibrate for 30 min before the optical spectrum was recorded. The concentration of the Zn(II)−quin-2 complex was determined by the change in absorption at 265 and 366 nm (absorbance maxima of quin-2) (*22*) following each addition of Zn(II), thus defining the extent of competition between the protein and the chelator. These data were fit using a competitive binding model in Dyna-Fit (*23*) to determine the zinc binding affinity, K_{Zn}, of each of the variant SmtBs. This model assumes two equivalent and independent zinc binding sites on the homodimer.

Tyrosine Fluorescence. Fluorescence intensity measurements were carried out using a SLM 4800 spectrofluorometer with an excitation wavelength of 280 nm (4 nm bandwidth) and an emission wavelength of 305 nm (16 nm bandwidth). Each variant of SmtB was diluted to 1.8 mL in buffer S to a final concentration of 4−7 μM. Following each *i*th addition of $ZnSO_4$ (2−5 μL) or buffer (for dilution and bleach corrections), the emission intensity was recorded as the average of four separate readings spaced 10 s apart and F_i/F_0 was determined, corrected for dilution, bleaching, and inner filter effects as derived from a mock titration of buffer into the protein sample essentially as described previously (*24*).

NMR Spectroscopy. NMR spectra were acquired on a Varian Unity Inova 500 MHz spectrometer in the Biomolecular NMR Laboratory at Texas A&M University. The sample contained 0.5 mM uniformly labeled ^{15}N-labeled S-methylated SmtB in 10 mM d_{18}-HEPES and 50 mM KCl (pH 6.0). Chemical shift referencing is relative to DSS (*25*). All spectra were processed and analyzed using NMRPipe (*26*) and SPARKY (*27*). The $^1H-^{15}N$ HSQC spectrum was recorded as a 160* × 512* two-dimensional (2D) matrix in the t_1 and t_2 dimensions, respectively, where *n** represents *n* complex points. Acquisition times in each dimension were 88.9 (t_1, ^{15}N) and 85.3 ms (t_2, $^1H^N$) defined by sweep widths of 1800 and 6000 Hz, respectively, for a total measurement time of 1.6 h. The data were apodized along t_1 by using a 90°-shifted sine bell, truncated at 9%, and along t_2 with a 90°-shifted squared sine bell, truncated at 1%. The data were zero-filled to digital resolutions of 5.6 (F_1) and 10 Hz (F_2). Δppm was calculated using the following relationship (*28*):

$$\Delta\text{ppm} = \sqrt{\Delta\delta_H^{\,2} + (^1/_7\Delta\delta_N)^2}$$

where δ_H is the chemical shift in the ^1H dimension and δ_N is the chemical shift in the ^{15}N dimension. Data for apo- and Zn_2 wild-type SmtB were obtained from the BioMagResBank (accession numbers 4128 and 4306, respectively) (*29*, *30*). Resonance assignments for S-methylated SmtB in the presence and absence of Zn(II) were inferred from comparison to the published 2D spectra of wild-type SmtB acquired under exactly the same solution conditions (*29*, *30*), provided the difference in chemical shift was ≤0.1 ppm.

RESULTS

Although there is not yet a crystallographic structure of Zn(II)- or Co(II)-substituted SmtB, two pairs of symmetry-related metal sites were inferred from Hg(II) complexes derived from mercuric acetate soaks of the apoprotein crystals (*9*). One pair of metal sites lies across the α5 helices, involving Asp104 and His106 from one monomer and His117′ and Glu120′ from the other, with the other pair at the peripheral tips of the dimer, near the α3 helices, and ligated by Cys61 and Asp64 (Figure 1). Previous studies revealed that Co(II) and Zn(II) bind to *one* pair of sites on the wild-type SmtB dimer (not *two* as predicted by the crystal structure) to form a chelate containing one to two thiolate ligands in a tetrahedral ligand field (*12*). Spectroscopic characterization of a series of SmtB cysteine and histidine substitution mutants was carried out here to determine which, if any, of these sites is occupied in solution by Co(II), used as a spectroscopic probe of the Zn(II) sites. SmtB contains three cysteine residues: Cys14 in the N-terminal "arm", a region of the protein not observed in the structure, Cys61 just N-terminal to the α3 helix, and Cys121, just C-terminal to the Hg(II) ion located between the α5 helices.

UV−Visible Absorption Spectra of Co(II)-Substituted Variant SmtBs. Complete corrected UV−vis electronic spectra are shown for a series of cysteine substitution (Cys → Ser) mutants of SmtB in Figure 2A. As can be seen, only Co(II)-substituted C121S SmtB is characterized by an absorption spectrum that is very similar to that of wild-type SmtB (*12*). This reveals that Cys121 does *not* play a primary role in the Co(II) coordination environment when Cys14 and Cys61 are both present.

When either Cys14 or Cys61 is substituted with nonliganding serine, the coordination environment remains tetrahedral, but each spectrum is characterized by an overall diminution in intensity, particularly in the near-ultraviolet region where $S^- \rightarrow$ Co(II) LMCT absorption occurs, coupled with a detectable blue shift in the ligand field transition region. These spectra are most consistent with the loss of one of the two primary sulfur donors in each case, specifically, Cys14 and Cys61, to the Co(II) bound in a site formed by ligands from the N-terminal arm and helix α3, denoted α3N. Given this situation, the double mutant, C14S/C61S SmtB, was expected to abolish Co(II) binding to this site, and eliminate all $S^- \rightarrow$ Co(II) LMCT absorption. Surprisingly, not only does C14S/C61S SmtB bind Co(II), the absorption spectrum is *identical* to that of C14S and C61S SmtBs (Figure 2A). Since Cys121 is the only thiolate ligand remaining in C14S/C61S SmtB, Cys121 must be part of the primary shell of metal ligands in this mutant. The excellent correspondence of the absorption spectra of Co(II)-substituted C14S, C61S, and C14S/C61S SmtBs further suggests that the thiolate ligand that remains in the C14S and C61S complexes is contributed by Cys121 as well, and not by Cys61 and Cys14, respectively. These spectra are fully consistent with Co(II) binding to the α5 interhelical site in C14S, C61S, and C14S/C61S SmtBs, into which Cys121 has been recruited (summarized in Figure 5 below). This makes the prediction that the substitution of Cys121 and Cys61 together would create a tetrahedral site composed exclusively of N and O ligands and devoid of thiolate ligands (cf. Figure 5); this is indeed the case (Figure 2A). The same Co(II) absorption spectrum characterizes C121S SmtB that was allowed to air-oxidize, thus forming a Cys14-S-S-Cys61′ intersubunit disulfide bond (Figure 3); this protein is still capable of binding Co(II) in a tetrahedral geometry (Figure

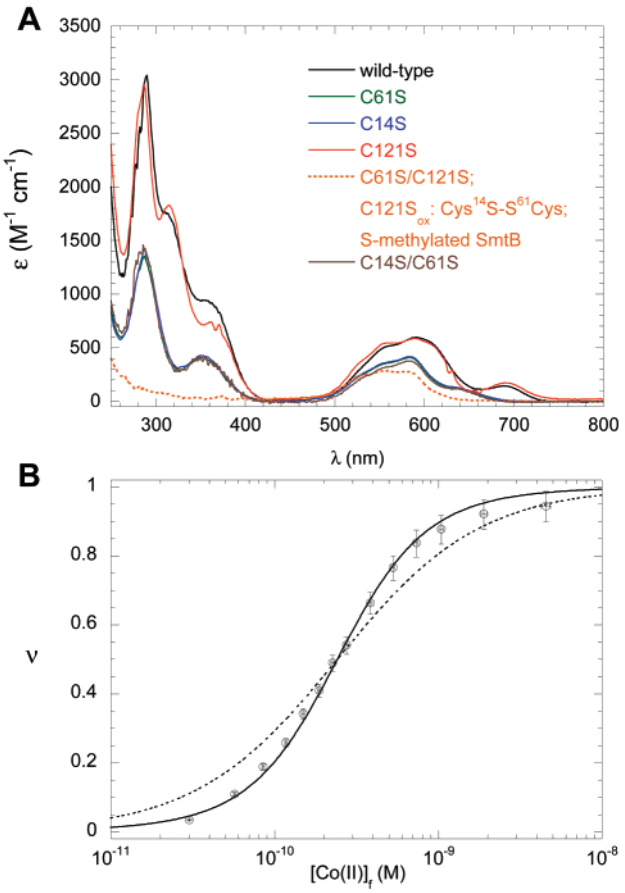

FIGURE 2: (A) Optical absorption spectra of wild-type SmtB and the various cysteine substitution mutants used in this study. Spectra are representative of a 1:1 Co(II):monomer stoichiometry. Data for wild-type SmtB are shown in black, C14S SmtB in blue, C61S SmtB in green, and C121S SmtB in red; data for C61S/C121S, $C121S_{ox}$:$Cys^{14}S$-$S^{61}Cys$, and S-methylated SmtBs are all shown in gold (all three have identical absorption spectra), and data for C14S/C61S SmtB are shown in silver. (B) Representative Co(II) binding isotherm obtained for 197 μM C14S SmtB in the presence of 1.1 mM EGTA. ν was calculated from A_{593} using an ϵ_{593} of 420 $\pm$ 20 M^{-1} cm^{-1} derived from multiple determinations. The dashed curve represents a nonlinear least-squares fit to a 1:1 binding model with a K_{Co} of 5.0 ($\pm$0.6) $\times$ 10^9 M^{-1}. The solid curve is a fit to a two-site cooperative binding model with a K_{int} of 1.6 ($\pm$0.1) $\times$ 10^9 M^{-1} and an ω of 7.1 $\pm$ 1.3. Here, macroscopic $K_1 = 2K_{int}$ and macroscopic $K_2 = K_{int}^2\omega$, where $\sqrt{K_2}$ is analogous to K_{Co} from the 1:1 binding model analysis. From these data, $\sqrt{K_2} = 4.3 \times 10^9$ M^{-1}. Conditions: 10 mM HEPES and 0.15 M KCl at pH 7.4.

2A). The same spectrum also characterizes an SmtB in which all of the cysteines have been derivatized with MMTS to form S-methylated SmtB (Figure 2A). As was found for C61S/C121S SmtB, S-methylated SmtB binds Co(II) with a stoichiometry of nearly 1:1 (metal:monomer) with very high affinity (Table 1).

Since all SmtB variants were found to bind Co(II), EGTA or NTA competition assays were carried out as previously described to determine the K_{Co} values for each of the SmtB derivatives described above (*12*). Figure 2B shows a representative titration for C14S SmtB with the results of these experiments listed in Table 1. Remarkably, although each of the SmtB variants of SmtB is devoid of particular cysteine residues, each binds Co(II) with an equilibrium affinity similar to that of the wild-type protein (Table 1).

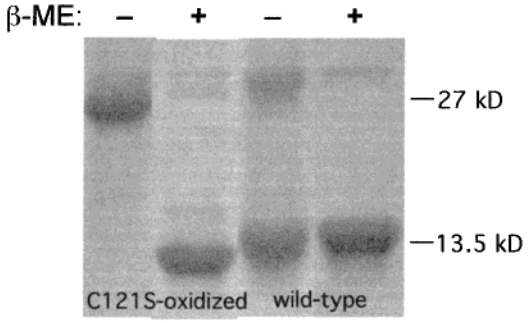

FIGURE 3: Denaturing SDS−PAGE analysis of air-oxidized C121S SmtB compared to wild-type SmtB electrophoresed in the absence (−) and presence (+) of 10 mM β-mercaptoethanol in the loading buffer. Wild-type SmtB runs as a monomer under both conditions, in contrast to air-oxidized C121S SmtB. Since C121S SmtB contains just two cysteines (Cys14 and Cys61), the crystallographic structure of apo-SmtB (*9*) strongly suggests that air-oxidized C121S SmtB would be capable of forming only a disulfide-cross-linked dimer between Cys14 of one subunit and Cys61′ of the other subunit (cf. Figure 1). The cross-linked dimer is readily reduced with 10 mM β-mercaptoethanol.

The Co(II) Spectrum of Wild-Type SmtB Is a Superposition of One Co(II) Bound to an α5 Site and One Bound to an α3N Site on the Dimer. Having determined that Co(II) binds preferentially to a site between the α5 helices when Cys14 and Cys61 are lost by substitution or derivatization, we made an attempt to disrupt the α5 site by introducing a His106 → Gln substitution, in which just one of the four proposed α5 ligands (Asp104, His106, His117′, and Glu120′) is converted to a nonliganding residue. If this protein bound Co(II), it would be expected to contain only the α3N metal binding site. Shown in Figure 4A is a superposition of the resulting absorption spectrum of Co(II)-substituted H106Q SmtB with that of wild-type and C61S SmtBs. The main envelope of the H106Q SmtB spectrum is red-shifted relative to that of wild-type SmtB but reflects a spectrum that remains tetrahedral, albeit distorted, with approximately one to two cysteines in the first shell of ligands, the latter based on the intensity at 320 nm (*31*). Remarkably, a simple sum of the Co(II) molar absorptivity spectra of H106Q SmtB, reflective of Co(II) bound to the α3N site, and C61S SmtB, reflective of Co(II) bound to the α5 site (in which Cys121 is recruited into the complex), essentially precisely recapitulates the experimental spectrum of Co(II)-substituted wild-type SmtB (*12*). Likewise, the absorption spectrum of Co(II)-substituted C121S SmtB is well-represented by a simple sum of Co(II)-substituted H106Q and S-methylated SmtBs (Figure 4B), and also accounts for the small but significant spectral differences (particularly at ≈370 nm) in the spectra of Co(II)-substituted wild-type and C121S SmtBs (Figure 2A). These data reveal that Co(II) binds to the SmtB homodimer in such a way that one Co(II) ion is bound to the α3N site and the other is bound in the α5 site, with the other two symmetry-related α3N and α5 sites on the dimer empty. This partitioning of Co(II) between the α3N and α5 sites is perhaps not surprising given their similar equilibrium affinities (K_{Co}) (Table 1).

Our interpretation of these Co(II) spectroscopic studies is summarized in Figure 5. In wild-type and C121S SmtBs, Co(II) partitions between one α3N and one α5 metal binding site. When one and/or the other strong thiolate ligand in the α3N site (Cys14 and/or Cys61) is lost by mutagenesis, Co-

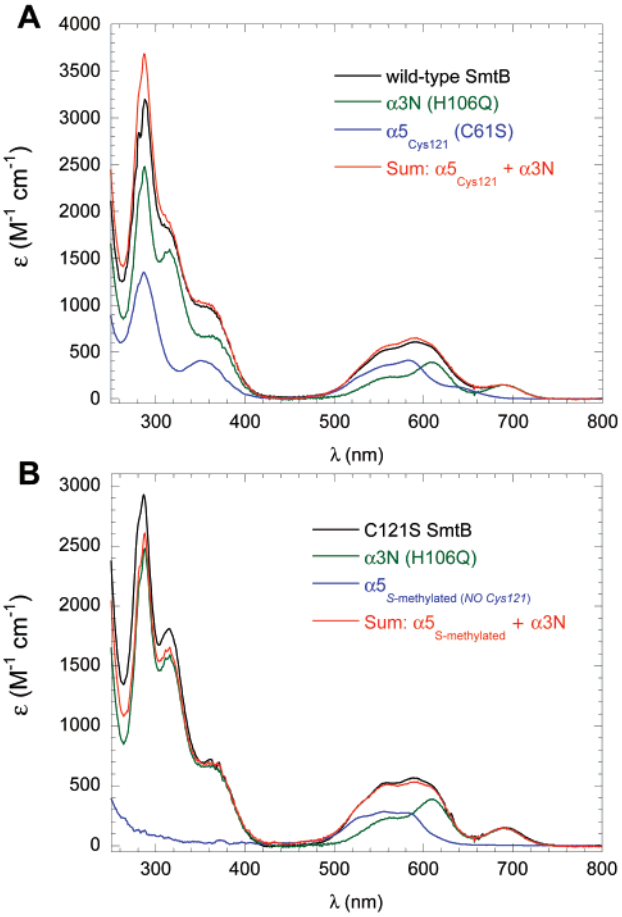

FIGURE 4: (A) Difference molar absorptivity spectra of Co(II)-substituted wild-type SmtB (black); H016Q SmtB, representative of Co(II) bound at the α3N site (green); C61S SmtB, representative of Co(II) bound at the α5 site, with Cys121 as a ligand (blue); and the calculated sum of the H106Q and C61S spectra (red). (B) Difference molar absorptivity difference spectra of Co(II)-substituted C121S SmtB (black); H016Q SmtB, representative of Co(II) bound at the α3N site (green); S-methylated SmtB, representative of Co(II) bound at the α5 site, with Cys121 as a ligand (blue); and the calculated sum of the H106Q and S-methylated SmtB spectra (red).

(II) binds exclusively to the metal sites between the α5 helices. This coordination complex appears to be capable of utilizing either Cys121 or Glu120 as a terminal metal ligand with essentially no effect on K_{Co} (Table 1). The experiments outlined below were carried out to determine K_{Zn} as well as to provide insight into whether Zn(II) might be characterized by a similar metal site partitioning on the homodimer.

Zn(II) Titrations of SmtB Variants in the Presence of Mag-fura-2. Previously, mag-fura-2 was employed to determine the stoichiometry of Zn(II) binding to wild-type SmtB and to define a lower limit to K_{Zn} (*12*). Similar experiments with each of the variant SmtBs were carried out to determine the extent to which cysteine substitution influenced Zn(II) binding. Figure 6 shows representative Zn(II) titrations of C14S and S-methylated SmtBs. The titration of C14S SmtB reveals that the C14S mutant binds 1 equiv of Zn(II) far tighter than mag-fura-2 followed by binding of ~0.7 equiv of Zn(II) with a K_{Zn} on the order of that of mag-fura-2. In contrast, S-methylated SmtB binds 0.7 equiv of Zn(II) with an affinity far greater than that of mag-fura-2 ($K_{Zn} \geq 10^{10}$ M^{-1}) (*12*). A stoichiometry of 0.7 suggests that some fraction of the S-methylated protein is inactive for metal binding; Co(II) studies with the same preparation of protein support this contention (data not shown).

Zn(II) Titrations of SmtB Variants in the Presence of Quin-2. Since only a lower limit for K_{Zn} for variant SmtBs could be obtained with the low-affinity indicator dye mag-fura-2, quin-2, a higher-affinity zinc chelator dye that forms a 1:1 complex with Zn(II) with a K_{Zn} of 2.7×10^{11} M^{-1} was used (*22*). Although complete equilibration of Zn(II) with quin-2/SmtB mixtures required >30 min under these conditions, equilibrium titrations could be obtained. Results from representative experiments are shown with wild-type (panel A) and C61S (panel B) SmtBs (Figure 7). Strikingly, K_{Zn} for wild-type SmtB appears to be too tight to determine accurately with only a lower limit for K_{Zn} of $\geq 10^{13}$ M^{-1} that can be defined by this experiment (Table 1). In contrast, K_{Zn} for the mutant SmtBs is easily determined from this competition assay. K_{Zn} for each of the α5 metal site variants tested is ≥20-fold lower than that of wild-type SmtB but still quite high (on the order of 10^{11} M^{-1}) (Table 1). Thus, although it is not known if Zn(II) partitions between the α3N and α5 sites in wild-type or C121S SmtB, the presence of an intact α3N site greatly increases the overall Zn(II) affinity by 1−2 orders of magnitude (Table 1).

Zn(II) Titrations of SmtB Variants As Monitored by Tyrosine Fluorescence Enhancement. SmtB contains four tyrosine residues, three of which are in the two-stranded β-sheet with one in the α5 helix (Tyr111) between the two α5 metal binding sites at the dimer interface. Although this experiment will report on changes in the overall fluorescence intensity, we reasoned that the fluorescence of Tyr111 would be greatly affected since this is the only tyrosine that is buried at the dimer interface. We reasoned that if at least one of the two Zn(II) ions binds to the α3N site in the wild-type SmtB versus solely the α5 sites in the cysteine substitution mutants, this might occur with significantly different changes in the total tyrosine fluorescence emission intensity. Figure 8 reveals that this is in fact the case. The maximal enhancement in tyrosine fluorescence intensity for wild-type SmtB is ≈7.5% (Figure 8A), while that for C61S, C61S/C121S, and S-methylated SmtBs is ≈11−12% (Figure 8A,B). Under these conditions (0.15 M KCl, pH 7.4, and 25 °C), all added Zn(II) will be bound to each of the proteins (Table 1). Although the effect is small, the shapes of the isotherms suggest that the binding of the first Zn(II) to the dimer causes most of the change in fluorescence intensity. In any case, the simple interpretation of these experiments is that Zn(II) binding to the cysteine mutants occurs at the same site (α5) and that this metal site is partially or fully distinct from that of the wild-type protein, results consistent with the Co(II) substitution data.

NMR Studies of S-Methylated SmtB. Since wild-type SmtB and S-methylated SmtB clearly harbor distinct Zn(II) binding sites, we used NMR perturbation spectroscopy to further pinpoint the location of these sites on the SmtB homodimer, with the underlying assumption that large changes in chemical shift directly report on Zn(II) binding. Since the amide backbone resonance assignments for wild-type SmtB in the presence and absence of Zn(II) are known (*29*, *30*), $^{15}N-^{1}H$ HSQC spectroscopy was used to catalog changes in the amide backbone chemical shifts for S-methylated SmtB in the presence and absence of stoichiometric Zn(II). The

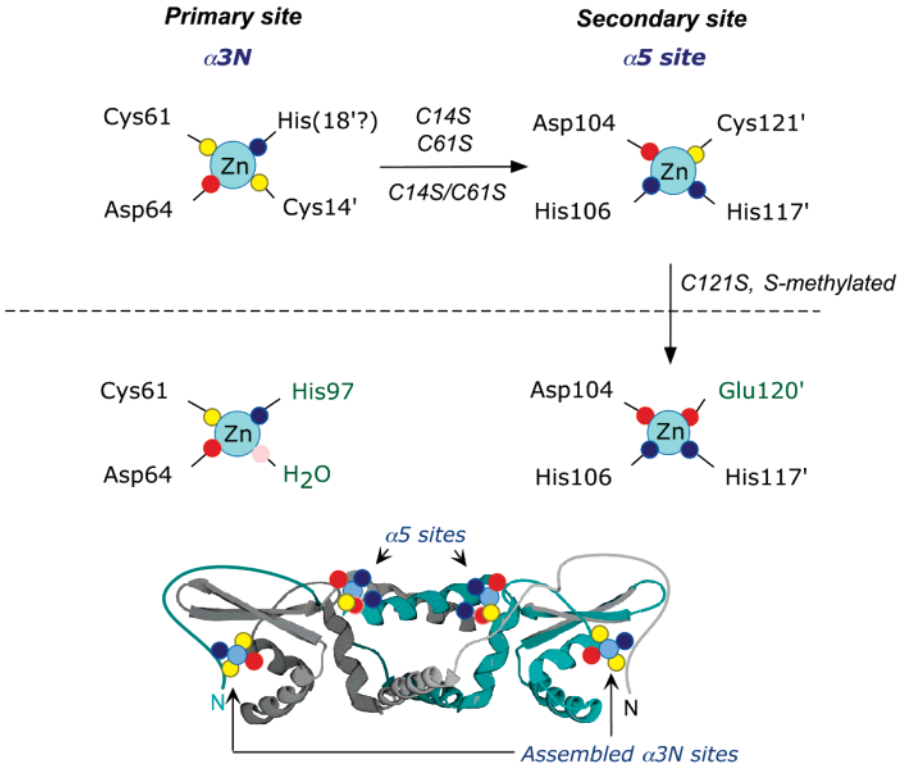

FIGURE 5: Models for Zn(II) and Co(II) binding sites in SmtB and mutant SmtBs. (Top) Models for the metal coordination complexes derived from Co(II) optical spectroscopy and Zn(II) and Co(II) X-ray absorption spectroscopy (*12*) and optical spectroscopy reported here (Figures 2 and 4). The α3N site is the primary Zn(II) binding site in wild-type SmtB in the absence of DNA. Mutagenesis of Cys14 and/or Cys61 destabilizes the α3N site and unmasks a metal binding site analogous to that found between the α5 helices in the crystallographic study (*9*) except that Cys121 is part of the primary coordination shell. Further substitution or derivatization of Cys121 creates the α5 sites observed in the crystallographic studies (*9*). (Middle) Metal binding sites inferred from mercuric acetate soaks of crystals of apo-SmtB. (Bottom) Both α3N and α5 sites are modeled onto the crystal structure of apo-SmtB with histidine residues represented as blue spheres, aspartates and glutamates in red, and cysteines in yellow.

Table 1: Equilibrium Association Constants for the Binding of Zn(II) (K_{Zn}) and Co(II) (K_{Co}) to SmtB Variants[a]

	K_{Zn} (M^{-1})[b]	K_{Co} (model 1) (M^{-1})[b]	K_{Co} (model 2) (M^{-1})[c]
wild type	$\geq 1 \times 10^{13}$	$1.7 (\pm 0.2) \times 10^9$	$1.1 (\pm 0.1) \times 10^9$
		α3N[d] $1.8 (\pm 0.4) \times 10^9$	$\omega = 2.3 \pm 0.2$
α5 (Cys121)			
C14S	$2.0 (\pm 1.0) \times 10^{11}$	$4.5 (\pm 0.1) \times 10^9$	$1.6 (\pm 0.1) \times 10^9$
	$[7.0 (\pm 1.4) \times 10^7]$[e]		$\omega = 7.1 \pm 1.3$
C61S	$5.0 (\pm 1.7) \times 10^{11}$	$4.3 (\pm 0.5) \times 10^9$	nd[f]
C14S/C61S	nd[f]	$5.2 (\pm 0.3) \times 10^9$	$2.0 (\pm 0.3) \times 10^9$
			$\omega = 6.7 \pm 1.8$
α5 (no Cys121)			
C61S/C121S	$3.5 (\pm 1.7) \times 10^{11}$	$4.8 (\pm 0.2) \times 10^9$	nd[f]
S-methylated	$7.9 (\pm 1.9) \times 10^{11}$	$1.5 (\pm 0.3) \times 10^9$	$5.3 (\pm 0.3) \times 10^8$
			$\omega = 8.1 \pm 0.8$

[a] Conditions: 25 °C, pH 7.4, and 0.15 M NaCl. [b] Resolved from fits to a 1:1 binding model (metal:monomer or two identical noninteracting sites per nondissociable dimer) in a quin-2 [Zn(II)], EGTA [Co(II)], or NTA [Co(II)] competition assay. [c] Resolved from fits to a 2:1 (metal:nondissociable dimer) cooperative binding model, in which the overall Co(II) binding affinity of the SmtB homodimer is defined by $K_{Co}^2\omega$, where ω is a unitless cooperativity parameter (*12*). [d] Calculated from the quotient $K_{Co}^2/K_{Co}^{S-methylated\ SmtB}$. [e] K_3 resolved from fits to a 3:1 (metal:nondissociable dimer) binding model where $K_1 = K_2 \neq K_3$. [f] Not determined.

results of this experiment are shown in Figure 9. They reveal that residues at or immediately adjacent to Cys14 in the N-terminal arm and Cys61 and Asp64 in the α3 helix are most strongly perturbed when Zn(II) is added to underivatized apo-SmtB, as would be expected for Zn(II) binding to the α3N site (cf. Figure 5). Strikingly, when these cysteines are S-methylated, major chemical shift perturbations cluster *only* in the α5 helix, with other changes largely common to both proteins. Thus, this perturbation analysis is consistent with metal loading at the α5 helices only. Since there is a subset of chemical shift changes that are common to both proteins, it cannot be concluded that Zn(II) binds exclusively to the α3N sites in wild-type SmtB, although the changes in chemical shift on metal binding are clearly largest here.

Facile Co(II) Equilibration between the α5 and α3N Metal Binding Sites upon Reduction of S-Methylated SmtB. Documentation of the distinct metal sites in the S-methylated SmtB versus wild-type SmtB prompted us to investigate whether Co(II) could rapidly equilibrate between the α5 and α3N sites upon reduction of the mixed disulfides in S-methylated SmtB with dithiothreitol. Figure 10 reveals that this in fact occurs. Prior to addition of dithiothreitol, the absorption

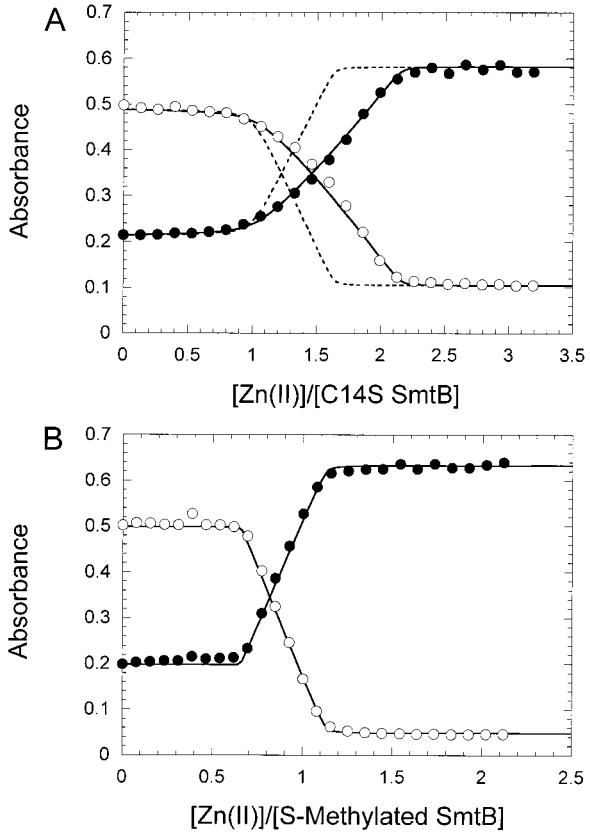

FIGURE 6: Representative titrations of Zn(II) into a mixture of mag-fura-2 and one of two variant SmtBs: (A) 26.1 μM C14S SmtB and 16.7 μM mag-fura-2 and (B) 36.1 μM total S-methylated SmtB and 16.8 μM mag-fura-2. In both panels, the filled circles represent A_{325} values, which are maximal in the Zn(II)−mag-fura-2 complex, and the empty circles represent A_{366} values, which are maximal in uncomplexed mag-fura-2. The solid lines represent nonlinear least-squares fits to the following models. For C14S SmtB, the data were fit as three metals binding to a nondissociable dimer with the following parameters: $[C14S]_{dimer} = 12.9$ μM (25.8 μM monomer), $K_1 = 5.1$ (±9.9) × 10^9 M^{-1}, $K_2 = 4.0$ (±2.7) × 10^9 M^{-1}, and $K_3 = 7.0$ (±1.4) × 10^7 M^{-1}. For illustration, a simulation with a 1:1 metal binding model (one metal per monomer or two per dimer) with K_{Zn} fixed at 1 × 10^{10} M^{-1} (dashed lines) does not adequately describe the data. (B) S-Methylated SmtB was fit to a 1:1 metal binding model with the following parameters: [active S-methylated SmtB monomer] = 25.3 μM (70% active), $K_1 = (7.0 \pm 670) \times 10^{12}$ M^{-1}. For both C14S and S-methylated SmtBs, K_1 and K_2 are meaningless since they are too tight to measure with this assay under these conditions. Conditions: 10 mM HEPES and 0.15 M KCl at pH 7.4 and 25 °C.

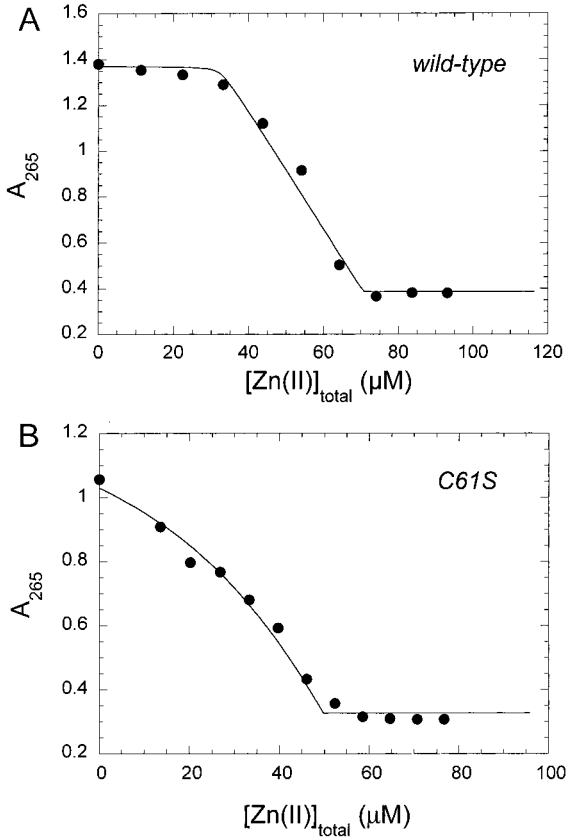

FIGURE 7: Representative titrations of Zn(II) into a mixture of quin-2 and one of two SmtB variants: (A) 35.1 μM wild-type SmtB and 32.5 μM quin-2 and (B) 37.2 μM C61S SmtB and 22.5 μM quin-2. The solid curve represents a nonlinear least-squares fit to a 1:1 binding model with K_{Zn} values of 1.0 × 10^{14} and 5.0 (±1.7) × 10^{11} M^{-1} for wild-type SmtB and C61S SmtB, respectively. Conditions: 10 mM HEPES and 0.15 M KCl at pH 7.4 and 25 °C.

spectrum of Co(II)-substituted S-methylated SmtB is reflective of binding only to the α5 helices and is devoid of any Co(II)−thiolate absorption. Upon addition of dithiothreitol, the spectrum red shifts and gains significant $S^- \rightarrow$ Co(II) intensity within the first shell of coordinating ligands. Not only does this occur rapidly (within 5 min), but the resulting spectrum shows features specifically characteristic of the α3N metal binding sites ($\lambda_{max} = 693$ nm) (Figure 4).

DISCUSSION

We show here that *Synechococcus* PCC7942 SmtB, the Zn(II)-sensing transcriptional regulator in cyanobacteria, harbors two structurally distinct pairs of metal binding sites, termed α3N and α5. The α3N site is assembled from ligands derived from the N-terminal unstructured arm (*9*) and the α3 helix. This metal binding site is structurally analogous to the tetrathiolate S_4 α3N site recently characterized in the Cd(II)/Pb(II) sensor CadC (*15*−*17*), but in SmtB is formed by two cysteines, one carboxylate ligand (possibly Asp64 in the α3 helix), and one imidazole ligand, hypothesized to be His18 (Figure 5), rather than four cysteines. We further propose that the Cys14/His18 and Cys61′/Asp64′ pairs are derived from different monomers, given that Cys14 and Cys61′ readily form an intersubunit disulfide bond (Figure 3). Although the identity of the histidine ligand in the α3N site as His18 is speculative, the side chain of His18 is within metal liganding distance of Cys61′ in the opposite subunit in a refined crystallographic structure of apo-SmtB determined to a higher resolution.[2] Unfortunately, attempts to test this spectroscopically have thus far failed since replacement of His18 with Cys results in quantitative formation of a stable disulfide bond between Cys18 and Cys14 and/or Cys61′.[3]

The proposed structure of the interhelical α5 coordination complex is fully compatible with a site composed of the α5 ligands as originally identified in the Hg(II) complex in the crystal structure (*9*), except that Cys121 is capable of donating a ligand to the Co(II) bound in the α5 site, possibly in place of Glu120 (Figure 5). This finding suggests that

[2] C. Eichen, M. VanZile, D. Giedroc, and J. Sacchettini, unpublished observations.

[3] M. VanZile, X. Chen, and D. Giedroc, unpublished observations.

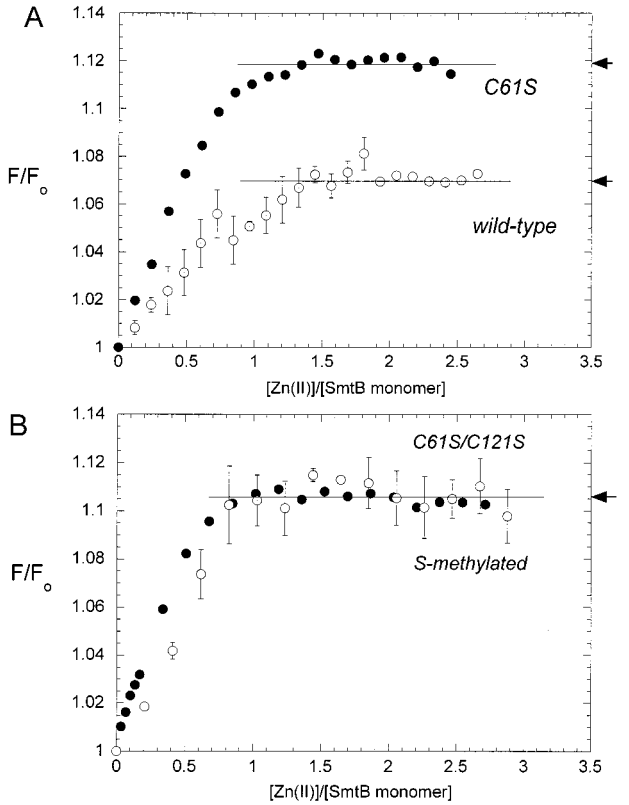

FIGURE 8: Enhancement of the intrinsic tyrosine fluorescence of various SmtBs as a function of added Zn(II). (A) Zn(II) binding isotherms obtained for C61S SmtB (●) vs wild-type SmtB (⊙). (B) Zn(II) binding isotherms obtained for C61S/C121S SmtB (●) vs S-methylated wild-type SmtB (⊙). The S-methylated protein used in these experiments contained ≈70% active molecules as determined by mag-fura-2 titration (Figure 6). The horizontal lines represent the maximum fluorescence enhancement obtained with each SmtB variant. Conditions: 10 mM HEPES and 0.15 M KCl at pH 7.4 and 25 °C.

the α5 site is somewhat flexible with respect to its coordination environment, in a way that has essentially no effect on the Co(II) binding affinity (see Table 1). Substitution of one of the four ligands in the proposed α5 chelate, His106, with a nonliganding side chain (Gln106) also results in a dramatic perturbation of the Co(II) spectrum of wild-type SmtB (Figure 4), effectively precluding metal binding to this site. On the other hand, substitution of His106 with Cys in the context of a triple Cys-to-Ser mutant (C14S/C61S/C121S SmtB) results in clear $S^- \rightarrow$ Co(II) LMCT absorption not present in the triple mutant itself, revealing that Cys can substitute for His at this position.[4] A sequence alignment (Figure 11) reveals that the proposed α5 site is strongly conserved across the ArsR/SmtB family, except for a putative CadC protein from *Listeria monocytogenes* (*32*) and ArsR from *Escherichia coli* plasmid R773, the latter of which is known to sense As(III) via the three clustered Cys residues in the α3 helix (*33*). We have recently characterized *L. monocytogenes* CadC and have shown that the spectral features attributed here to a Co(II)−α5 metal complex are completely and uniquely lost in this CadC (*17*). In addition, if one makes further allowances for substitution of proposed metal ligands with other metal liganding amino acids (Cys, His, Asp, and Glu), the basic structure of the α3N site is also conserved in a subset of ArsR/SmtB proteins (Figure 11).

Co(II) exhibits the remarkable property of partitioning nearly precisely between one of the two available α3N and α5 sites on the wild-type and C121S SmtB homodimers, to an extent largely in accord with their equilibrium affinities (Table 1), with the other two symmetry-related sites remaining empty on the dimer. Thus, Co(II) binds with weak positive cooperativity to the two structurally nonequivalent sites (*12*), followed by strong negative cooperativity of loading at the other two symmetry-related sites. This partitioning characteristic of Co(II) may also be characteristic of Ni(II) as well (*12*). At low Ni(II) concentrations, optical spectroscopy and Ni(II) XAS reveal that Ni(II) binds to apo-SmtB in an octahedral coordination geometry before adopting a geometry characterized by a lower coordination number and at least one thiolate ligand as more Ni(II) is added (*12*). It is tempting to speculate that Ni(II) binds first to a site containing some or all of the α5 ligands before moving to an α3N-like site with excess Ni(II). These binding properties of Ni(II) and Co(II) appear to be readily distinguished from those Zn(II), which appears to bind preferentially to the thiolate-containing α3N sites. Although the origin of this apparent selectivity is unknown, it might be partially explained by the more thiophilic nature of Zn(II) versus Co(II) and Ni(II).

We also show that Co(II) bound exclusively to the α5 metal binding sites rapidly equilibrates between the α3N and α5 sites upon reduction of the mixed disulfide bonds in S-methylated SmtB, despite the fact that the binding is very tight at equilibrium at both sites. Although it is not yet known if this result is reporting on true intramolecular migration or transfer, such a pathway could be facilitated by ligand exchange with one or both ligands, e.g., Cys14, derived from one of the flexible N-terminal domains in the dimer. It seems unlikely that Zn(II) also partitions between the α3N and α5 sites, since K_{Zn} for wild-type SmtB is at least 20-fold larger than those for any of the SmtBs that contain only an intact α5 site. Thus, in the absence of DNA, Zn(II) would appear to be bound exclusively to the peripheral α3N sites, in contrast to Co(II). The binding of Zn(II) and the binding of Co(II) to wild-type SmtB can also be distinguished from one another by isothermal titration calorimetry.[5] What seems to be common to both Zn(II) and Co(II) [and perhaps Ni(II)] binding is that only two of the four available α3N and α5 metal sites can be loaded with metal at any one time since the stoichiometry of metal binding is always 1:1 (metal:monomer or two per dimer) as revealed by optical spectroscopy (*12*) and isothermal titration calorimetry.[5] This is in contrast to *S. aureus* pI258 CadC (*17*) and *Synechocystis* ZiaR,[6] both of which contain structurally intact α3N and α5 metal sites that are capable of binding Zn(II) [or Co(II)] simultaneously. The structural origin of this strong negative cooperativity of metal binding in SmtB is not known but suggests that once two metals are loaded, the symmetry of

[4] Substitution of His106 with Cys in the context of a triple Cys → Ser mutant protein (C14S/C61S/H106C/C121S) gives a Co(II) visible absorption spectrum which reveals direct metal coordination by Cys106 in the α5 metal binding site (X. Chen and D. Giedroc, unpublished observations).

[5] M. L. VanZile and D. P. Giedroc, manuscript in preparation.

[6] L. Busenlehner and D. Giedroc, unpublished results.

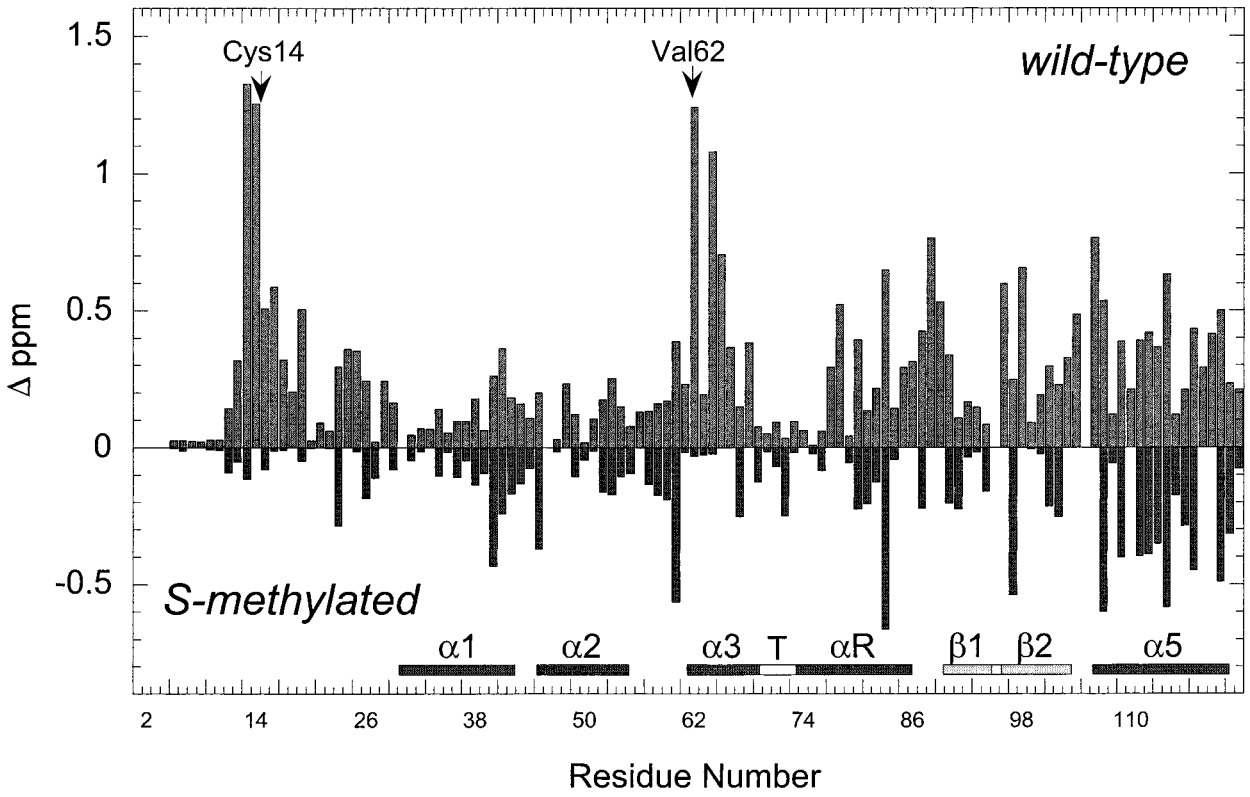

FIGURE 9: Chemical shift perturbations induced in ^{15}N-labeled wild-type SmtB vs ^{15}N-labeled S-methylated SmtB upon addition of Zn(II). Δppm was calculated from ^{15}N HSQC spectra as described in Materials and Methods. Values for S-methylated SmtB were multiplied by −1 to facilitate comparison with those of underivatized SmtB. SmtB contains proline residues at positions 4, 30, and 46; the other gaps in each bar plot represent places where unambiguous resonance assignments could not be obtained.

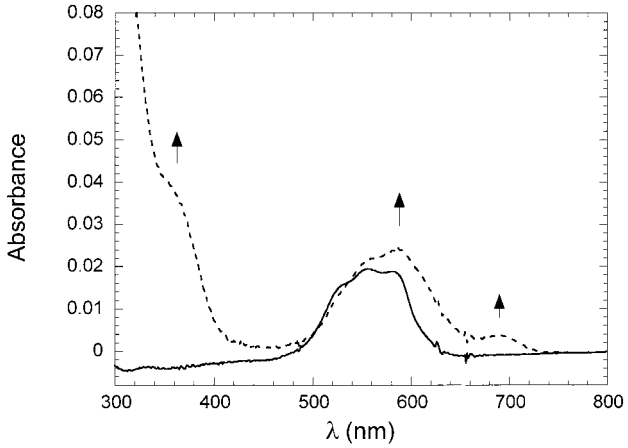

FIGURE 10: Rapid equilibration of Co(II) to the wild-type superposition of α5 and α3N sites from the α5 site in S-methylated SmtB upon addition of dithiothreitol: 66.5 μM Co(II)$_1$ S-methylated SmtB [one Co(II) per monomer protein] (—) compared to that following the addition of 17 mM DTT and incubation for 5 min (•••). Conditions: 10 mM HEPES and 0.15 M KCl at pH 7.4 and 25 °C.

the dimer is strongly disrupted. This unusual property may be important for SmtB in performing its function, upon which the following paper expands (*14*).

The affinity of the α3N and α5 metal binding sites in SmtB for Zn(II) is extremely high at equilibrium (Table 1) and is of an order of magnitude similar to that which characterizes structural (*34*, *35*) and catalytic (*36*) sites in zinc metalloproteins. K_{Zn} appears to be incompatible with early expectations that the affinity of a metalloregulatory site would be appropriately tuned by the intracellular fluxes of free metal ion over which regulation of gene expression would occur (*3*) since K_{Zn} for both α5 or α3N sites in SmtB (*14)* predicts free zinc fluxes in the picomolar range (*37*). Although more work is required, our results are consistent with the idea that zinc metalloregulation of *smt* expression in cyanobacteria is under kinetic rather than thermodynamic control as previously hypothesized by O'Halloran and coworkers for *E. coli* Zur and ZntR, two zinc metalloregulatory proteins whose transcriptional regulatory response occurs over the femtomolar range in free Zn(II) (*37*). Indeed, as a general rule, metal sensor sites might be distinguished from structural and catalytic metal sites by distinct kinetic labilities rather than different thermodynamic stabilities. It is interesting to note that both the α3N and α5 sites are found near the surface of SmtB, where ligand exchange might be readily accommodated.

As pointed out above, the presence of two metal binding sites on SmtB is not unique within the ArsR/SmtB family of metalloregulatory sensor proteins. If one examines a sequence alignment of several of the members of the ArsR/SmtB family, several additional points stand out (Figure 11). First, all family members that contain an α5 site composed of the four proposed α5 ligands, including SmtB (*34*), *S. aureus* CzrA (*18*), *Synechocystis* ZiaR (*19*), and *S. aureus* pI258 CadC (*16*), all respond to zinc. It is therefore tempting to speculate that the primary role of the α5 site is to sense Zn(II), and at least in one case Co(II) (*18*), two borderline hard/soft ions with similar ionic radii that often adopt tetrahedral or distorted tetrahedral geometries in proteins. The α3N site, on the other hand, may be responsible for sensing larger, softer thiophilic metals, including Cd(II),

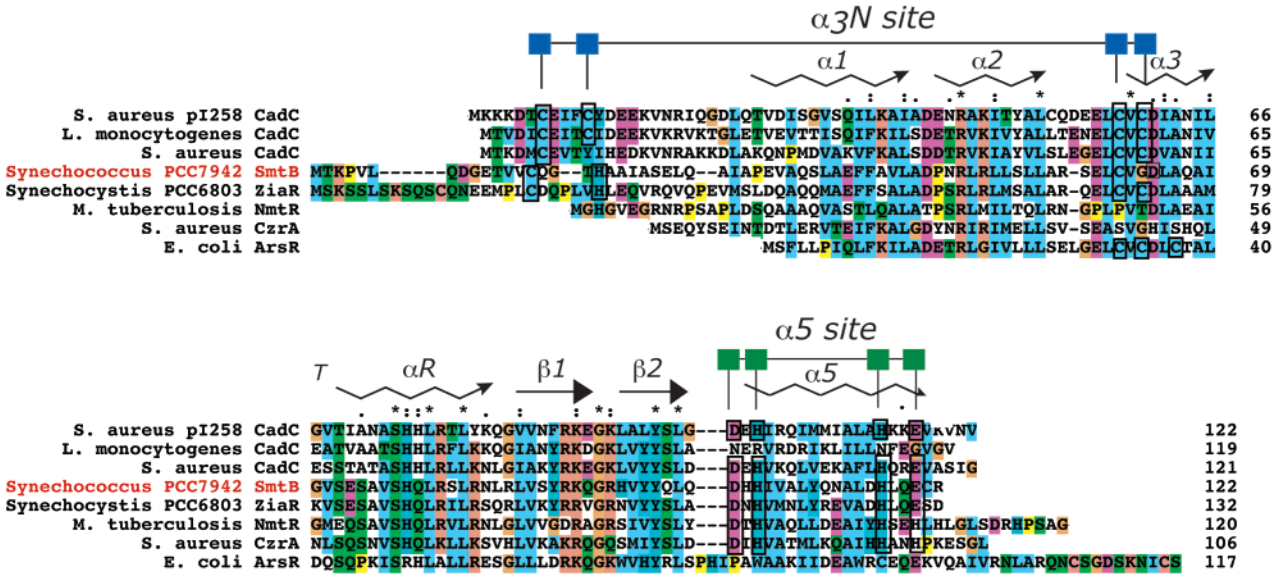

FIGURE 11: Sequence alignment of the ArsR/SmtB superfamily of metalloregulatory transcriptional repressors. The proposed α3N site and the α5 site are denoted with the secondary structure of apo-SmtB schematically indicated above the sequences. The sequence alignment shown was generated using ClustalX (http://www-igbmc.u-strasbg.fr/BioInfo/). *S. aureus* pI258 CadC (P20047), *L. monocytogenes* CadC (Q56405), *S. aureus* CadC (P37374), *Synechococcus* sp. PCC7942 SmtB (P30340), *Synechocystis* sp. PCC6803 ZiaR (Q55940), *Mycobacterium tuberculosis* NmtR (NP_218261.1), *S. aureus* CzrA (O85142), and *E. coli* R773 ArsR (P15905) are shown (Swiss-Prot, TrEMBL, and Genbank accession numbers are in parentheses). The boxed residues are conserved metal binding residues. The amino acid residues are color-coded as follows: blue, ionizable aromatic; light blue, nonpolar aliphatic; green, polar neutral; orange, basic; purple, acidic; yellow, proline; and brown, glycine.

Bi(III), and Pb(II) (*16*, *17*), with the α3 site of ArsR selective for smaller thiophilic ions such as As(III) and Sb(III) (*33*). Experiments with *S. aureus* pI258 CadC (*15*−*17*) and *S. aureus* CzrA[7] are consistent with this hypothesis. The following paper (*14*) examines in detail the complex DNA binding properties of SmtB and elucidates the degree to which the α3N and α5 metal sites are responsible for metal sensing and allosteric regulation of *smt* O/P binding.

REFERENCES

1. Coleman, J. E. (1992) *Annu. Rev. Biochem. 61*, 897−946.
2. Vallee, B. L., and Fallchuk, K. H. (1993) *Physiol. Rev. 73*, 79−118.
3. O'Halloran, T. V. (1989) in *Metal ions in biological systems, Vol. 25, Interrelations among metal ions, enzymes, and gene expression* (Sigel, H., and Sigel, A., Eds.) pp 105−146, Marcel Dekker, New York and Basel.
4. O'Halloran, T. V. (1993) *Science 261*, 715−725.
5. Shi, W., Wu, J., and Rosen, B. P. (1994) *J. Biol. Chem. 269*, 19826−19829.
6. Robinson, N. J., Bird, A. J., and Turner, J. S. (1998) in *Metal ions in gene regulation* (Silver, S., and Walden, W., Eds.) pp 372−397, Chapman and Hall, New York.
7. Daniels, M. J., Turner-Cavet, J. S., Selkirk, R., Sun, H., Parkinson, J. A., Sadler, P. J., and Robinson, N. J. (1998) *J. Biol. Chem. 273*, 22957−22961.
8. Blindauer, C. A., Harrison, M. D., Parkinson, J. A., Robinson, A. K., Cavet, J. S., Robinson, N. J., and Sadler, P. J. (2001) *Proc. Natl. Acad. Sci. U.S.A. 98*, 9593−9598.
9. Cook, W. J., Kar, S. R., Taylor, K. B., and Hall, L. M. (1998) *J. Mol. Biol. 275*, 337−346.
10. Huckle, J. W., Morby, A. P., Turner, J. S., and Robinson, N. J. (1993) *Mol. Microbiol. 7*, 177−187.
11. Kar, S. R., Adams, A. C., Lebowitz, J., Taylor, K. B., and Hall, L. M. (1997) *Biochemistry 36*, 15343−15348.
12. VanZile, M. L., Cosper, N. J., Scott, R. A., and Giedroc, D. P. (2000) *Biochemistry 39*, 11818−11829.
13. Turner, J. S., Glands, P. D., Samson, A. C. R., and Robinson, N. J. (1996) *Nucleic Acids Res. 19*, 3714−3721.
14. VanZile, M. L., Chen, X., and Giedroc, D. P. (2002) *Biochemistry 41*, 9776−9786.
15. Busenlehner, L. S., Cosper, N. J., Scott, R. A., Rosen, B. P., Wong, M. D., and Giedroc, D. P. (2001) *Biochemistry 40*, 4426−4436.
16. Busenlehner, L. S., Apuy, J. L., and Giedroc, D. P. (2002) *J. Biol. Inorg. Chem. 7*, 551−559.
17. Busenlehner, L. S., Weng, T.-C., Penner-Hahn, J. E., and Giedroc, D. P. (2002) *J. Mol. Biol. 319*, 685−701.
18. Xiong, A., and Jayaswal, R. K. (1998) *J. Bacteriol. 180*, 4024−4029.
19. Thelwell, C., Robinson, N. J., and Turner-Cavet, J. S. (1998) *Proc. Natl. Acad. Sci. U.S.A. 95*, 10728−10733.
20. Qiu, H., Kodadek, T., and Giedroc, D. P. (1994) *J. Biol. Chem. 269*, 2773−2781.
21. Walkup, G. K., and Imperiali, B. (1997) *J. Am. Chem. Soc. 119*, 3443−3450.
22. Jefferson, J. R., Hunt, J. B., and Ginsburg, A. (1990) *Anal. Biochem. 187*, 328−336.
23. Kuzmic, P. (1996) *Anal. Biochem. 237*, 260−273.
24. Giedroc, D. P., Khan, R., and Barnhart, K. (1990) *J. Biol. Chem. 265*, 11444−11455.
25. Wishart, D. S., Bigam, C. G., Yao, J., Abildgaard, F., Dyson, H. J., Oldfield, E., Markley, J. L., and Sykes, B. D. (1995) *J. Biomol. NMR 6*, 135−140.
26. Delaglio, F., Grzesiek, S., Vuister, G. W., Zhu, G., Pfeifer, J., and Bax, A. (1995) *J. Biomol. NMR 6*, 277−293.
27. Goddard, T. D., and Kneller, D. G. *SPARKY 3*, University of California, San Francisco (unpublished data).
28. Williamson, R. A., Carr, M. D., Frenkial, T. A., Fenney, J., and Freedman, R. B. (1997) *Biochemistry 36*, 13882−13889.
29. Morita, E. H., Kosada, T., Yamazaki, T., Kyogoku, Y., and Hayashi, H. (1998) *J. Biomol. NMR 12*, 453−454.
30. Kosada, T., Morita, E. H., Miura, A., Yamazaki, T., Hayashi, H., and Kyogoku, Y. (1999) *J. Biomol. NMR 14*, 191−192.
31. Henehan, C. J., Pountney, D. L., Zerbe, O., and Vasak, M. (1993) *Protein Sci. 2*, 1756−1764.
32. Lebrun, M., Audurier, A., and Cossart, P. (1994) *J. Bacteriol. 176*, 3040−3048.
33. Shi, W., Dong, J., Scott, R. A., Ksenzenko, M. Y., and Rosen, B. P. (1996) *J. Biol. Chem. 271*, 9291−9297.
34. Guo, J., and Giedroc, D. P. (1997) *Biochemistry 36*, 730−742.

[7] M. Pennella, C. Eichen, J. Sacchettini, and D. P. Giedroc, unpublished results.

35. Krizek, B. A., Amann, B. T., Kilfoil, V. J., Merkle, D. L., and Berg, J. M. (1991) *J. Am. Chem. Soc. 113*, 4518−4523.
36. Fierke, C. A., Maliwal, B. P., and Feliccia, V. L. (1998) *Anal. Chem. 70*, 4717−4723.
37. Outten, C. E., and O'Halloran, T. V. (2001) *Science 292*, 2488−2492.

BI0201771